Structural Engineering and Mechanics, Vol. 6, No. 8 (1998) 921-937
DOI: http://dx.doi.org/10.12989/sem.1998.6.8.921

A four-node degenerated shell element with drilling degrees of freedom

Ji Hun Kim† and Byung Chai Lee‡

Department of Mechanical Engineering, Korea Advanced Institute of Science and Technology, 373-1, Kusong-dong, Yusung-gu, Taejon 305-701, Korea

Abstract. A new four-node degenerated shell element with drilling degrees of freedom (DOF) is proposed. Allman-type displacement approximation is incorporated into the formulation of degenerated shell elements. The approximation improves in-plane performance and eliminates singularities of system matrices resulted from DOF deficiency. Transverse shear locking is circumvented by introducing assumed covariant shear strains. Two kinds of penalty energy are considered in the formulation for the purpose of suppressing spurious modes and representing true drilling rotations. The proposed element can be applied to almost all kinds of shell problems including composite laminated shell structures and folded shell structures. Numerical examples show that the element is of good accuracy and of reasonably fast convergence rate.

Key words: degenerated shell element; drilling DOF; Allman-type displacement approximation; composite laminated shell structures; folded structures; true drilling rotation.

1. Introduction

Degenerated shell elements have been used widely for analyses of shell structures since Ahmad *et al.* (1970). It is mainly because of their features such as good performance, relative efficiency, versatility of treating variable thickness and composite laminated structures, and extensibility to geometric and material nonlinear problems. The degenerated shell element usually gives good results for moderately thick shells, but the results deteriorate rapidly as the shell becomes thinner (Zienkiewicz *et al.* 1971). The phenomenon is referred to locking. A lot of methods for resolving the locking phenomenon have been proposed and applied to degenerated shell elements. One of the most successful methods is the assumed strain method. Lately, many good shell elements adopting the assumed strain method were developed (Bathe and Dvorkin 1986, Park and Stanley 1986, Huang and Hinton 1986, Jang and Pinsky 1987, Choi and Paik 1994, etc.). It seems that shell elements developed by Bathe and Dvorkin (1986) or Choi and Paik (1994) are among the best available four-node degenerated shell elements. But they have only five degrees of freedom (DOF) for all nodes and their in-plane shear performances are not so good for distorted meshes. The five DOF shell element results in inconveniences that the system would be singular in the case of coplanar elements layout.

In-plane performance can be improved by including either non-conforming modes,

† Ph.D. Student
‡ Associate Professor

enhanced assumed strains and hybrid stress fields, or drilling DOF. But, shell elements of six DOF per node can be made only by introducing drilling DOF. Allman (1984) developed a triangular membrane element with drilling DOF. A lot of studies have been followed to extend and improve the membrane element empirically and theoretically. Ibrahimbegovic *et al.* (1990), MacNeal and Harder (1988), and Choi and Lee (1995) studied for more rational formulation of membrane elements with drilling DOF. Yunus and Pawlak (1991), Sze and Ghali (1993), and Choi *et al.* (1996) developed solid elements with full rotational DOF. Aminpour (1992), Cook (1994), and Sze *et al.* (1997) proposed shell elements with drilling DOF.

In this paper, it is shown that the Allman-type displacement approximation (Allman 1984) can be extended to three dimensional space based on the beam theory. Using the approximation, new displacement fields of a four-node degenerated shell element with drilling DOF are derived from those of an eight-node element. The assumed strain method (Choi and Paik 1994) is adopted to circumvent the transverse shear locking. Conventional steps of calculating stiffness matrices are followed and a 2×2 Gaussian quadrature is used. Through-thickness numerical integration is included in the formulation for the analysis of composite laminated shells (Panda and Natarajan 1981). Since the element exhibits two spurious modes, two kinds of penalty energy (Kanok-Nukulchai 1979, MacNeal and Harder 1988) are considered. It is shown through numerical examples that the penalty energies do not deteriorate the element performance. The results of numerical tests are presented to demonstrate the good performance of the proposed element.

2. Element geometry and kinematics

2.1. Element geometry

Schemes of displacement interpolation can be derived easily from geometry interpolation. Initial geometry of a typical degenerated shell element is represented by the coordinates of all points within the element as follows.

$$\begin{Bmatrix} x \\ y \\ z \end{Bmatrix} = \sum_{k=1}^{n} N_k(\xi,\ \eta) \begin{Bmatrix} x_k \\ y_k \\ z_k \end{Bmatrix}_{mid} + \sum_{k=1}^{n} N_k(\xi,\ \eta)\frac{\zeta h_k}{2} \begin{Bmatrix} \bar{V}_{3k}^{x} \\ \bar{V}_{3k}^{y} \\ \bar{V}_{3k}^{z} \end{Bmatrix} \tag{1}$$

where n is the number of nodes in an element, $N_k(\xi,\ \eta)$ are shape functions corresponding to the surface ζ=constant, h_k, is the thickness of the shell at node k, $(x_k,\ y_k,\ z_k)$ are the global coordinates of node k, $(\xi,\ \eta,\ \zeta)$ are the natural coordinates, and $\{\bar{V}_{3k}^{x},\ \bar{V}_{3k}^{y},\ \bar{V}_{3k}^{z}\}^T$ is the unit normal vector at node k as shown in Fig. 1.

2.2. Kinematics

A typical degenerated shell element has five degrees of freedom at each node, which are three displacements $(u_k,\ v_k,\ w_k)$ and two rotations $(\alpha_{1k},\ \alpha_{2k})$. Since two rotations $(\alpha_{1k},\ \alpha_{2k})$ in

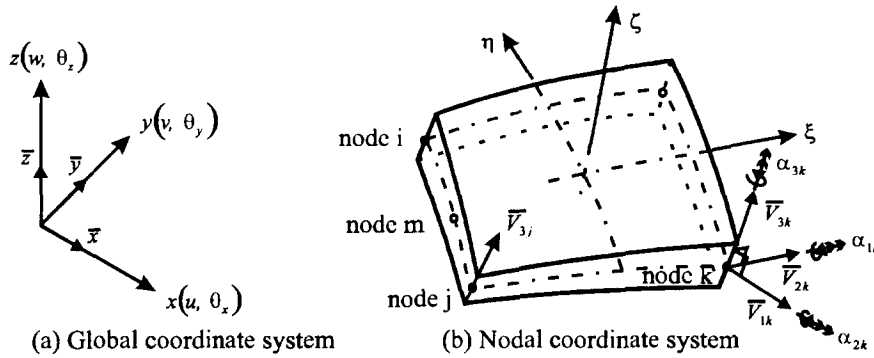

(a) Global coordinate system (b) Nodal coordinate system

Fig. 1 Element geometry and coordinate systems

the local coordinate system can be related to the rotations (θ_{xk}, θ_{yk}, θ_{zk}) in the global coordinate system if the rotations are small, the displacement fields of the eight-node degenerated shell element are written as

$$\{u\} = [N]_{S8}\{\delta\}_{S8} \tag{2}$$

where

$$\{u\} = \{u \ v \ w\}^T,$$

$$[N]_{S8} = \begin{bmatrix} & N_k & 0 & 0 & 0 & \overline{N}_k\overline{V}^z_{3k} & -\overline{N}_k\overline{V}^y_{3k} & \\ \cdots & 0 & N_k & 0 & -\overline{N}_k\overline{V}^z_{3k} & 0 & \overline{N}_k\overline{V}^x_{3k} & \cdots \\ & 0 & 0 & N_k & \overline{N}_k\overline{V}^y_{3k} & -\overline{N}_k\overline{V}^x_{3k} & 0 & \end{bmatrix},$$

$$\overline{N}_k = N_k\zeta\frac{h_k}{2},$$

$$\{\delta\}_{S8} = \{u_1 \ v_1 \ w_1 \ \theta_{x1} \ \theta_{y1} \ \theta_{z1} \ u_2 \cdots \ \theta_{z8}\}^T$$

2.3. The mid-side displacement approximation

Let us consider a four-node shell element which has straight edges and an eight-node element of the same shape and size which has mid-side nodes on the center of each edge. We assume that the edge behaves like a beam and the beam has the local coordinate system as shown in Fig. 2. If transverse shear strains of the beam are constant, the two displacement components normal to the beam axis are approximated quadratic, and the axial displacement and three rotations are approximated linear, the displacement fields in the beam are given in terms of 12 unknowns as follows:

$$u' = a_0 + a_1 s + a_2 s^2 \tag{3a}$$

$$v' = b_0 + b_1 s + b_2 s^2 \tag{3b}$$

$$w' = c_0 + c_1 s \tag{3c}$$

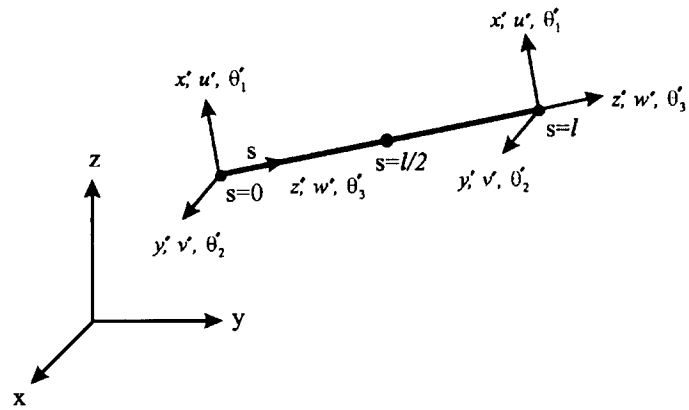

Fig. 2 The edge of a shell element

$$\theta_1' = -\frac{dv'}{ds} + \gamma_2,\quad \theta_2' = \frac{du'}{ds} - \gamma_1,\quad \theta_3' = d_0 + d_1 s \tag{3d, 3e, 3f}$$

where s is the coordinate along the beam axis, γ_1 and γ_2 are the constant transverse shear strains. The unknown coefficients in Eqs. (3a) to (3f) can be related to the displacement components at both ends of the beam. With the end displacement components

$$u_i',\ v_i',\ w_i',\ \theta_{1i}',\ \theta_{2i}',\ \theta_{3i}',\quad \text{at } s = 0 \tag{4a}$$

$$u_j',\ v_j',\ w_j',\ \theta_{1j}',\ \theta_{2j}',\ \theta_{3j}',\quad \text{at } s = l \tag{4b}$$

Eqs. (3a) to (3f) can be solved simultaneously. And the approximated displacement fields of the beam are given as

$$u' = u_i' + \left[\frac{1}{2}(\theta_{2i}' - \theta_{2j}') + \frac{1}{l}(u_j' - u_i')\right]s - \frac{1}{2l}(\theta_{2i}' - \theta_{2j}')\,s^2 \tag{5a}$$

$$v' = v_i' + \left[-\frac{1}{2}(\theta_{1i}' - \theta_{1j}') + \frac{1}{l}(v_j' - v_i')\right]s + \frac{1}{2l}(\theta_{1i}' - \theta_{1j}')\,s^2 \tag{5b}$$

$$w' = w_i' + \frac{1}{l}(w_j' - w_i')s,\quad \theta_1' = -\frac{1}{l}(\theta_{1i}' - \theta_{1j}')\,s + \theta_{1i}' \tag{5c, 5d}$$

$$\theta_2' = -\frac{1}{l}(\theta_{2i}' - \theta_{2j}')\,s + \theta_{2i}',\quad \theta_3' = -\frac{1}{l}(\theta_{3i}' - \theta_{3j}')\,s + \theta_{3i}' \tag{5e, 5f}$$

The mid-side node displacements at the center node m in the global coordinate system are obtained by substituting $s=l/2$ and transforming coordinate systems as follows

$$u_m = \frac{1}{2}(u_i + u_j) + y_{ji}(\theta_{zj} - \theta_{zi}) - z_{ji}(\theta_{yj} - \theta_{yi}) \tag{6a}$$

$$v_m = \frac{1}{2}(v_i + v_j) + z_{ji}(\theta_{xj} - \theta_{xi}) - x_{ji}(\theta_{zj} - \theta_{zi}) \tag{6b}$$

$$w_m = \frac{1}{2}(w_i + w_j) + x_{ji}(\theta_{yj} - \theta_{yi}) - y_{ji}(\theta_{xj} - \theta_{xi}) \tag{6c}$$

$$\theta_{xm} = \frac{1}{2}(\theta_{xi} + \theta_{xj}), \quad \theta_{ym} = \frac{1}{2}(\theta_{yi} + \theta_{yj}), \quad \theta_{zm} = \frac{1}{2}(\theta_{zi} + \theta_{zj}) \tag{6d, 6e, 6f}$$

where $x_{ji} = (x_j - x_i)/8$, $y_{ji} = (y_j - y_i)/8$, $z_{ji} = (z_j - z_i)/8$.

2.4. New displacement field including the drilling DOF

Using the Eqs. (6a) to (6f), we can relate the displacement fields of a four-node, 24 DOF shell element to those of an eight-node, 40 DOF shell element. We denote the relation concisely as follows.

$$\{\delta\}_{S8} = [T]_{SR}\{\delta\}_{S4} \tag{7}$$

where

$$[T]_{SR} = \begin{bmatrix} & [I]_{24\times24} & & \\ [T_{12}^1] & [T_{12}^2] & [0]_{6\times6} & [0]_{6\times6} \\ [0]_{6\times6} & [T_{23}^1] & [T_{23}^2] & [0]_{6\times6} \\ [0]_{6\times6} & [0]_{6\times6} & [T_{34}^1] & [T_{34}^2] \\ [T_{41}^2] & [0]_{6\times6} & [0]_{6\times6} & [T_{41}^1] \end{bmatrix},$$

$$[T_{ij}^1] = \begin{bmatrix} \frac{1}{2}[I]_{3\times3} & [L_{ij}] \\ [0]_{3\times3} & \frac{1}{2}[I]_{3\times3} \end{bmatrix}, \quad [T_{ij}^2] = \begin{bmatrix} \frac{1}{2}[I]_{3\times3} & -[L_{ij}] \\ [0]_{3\times3} & \frac{1}{2}[I]_{3\times3} \end{bmatrix}, \quad [L_{ij}] = \begin{bmatrix} 0 & z_{ji} & -y_{ji} \\ -z_{ji} & 0 & x_{ji} \\ y_{ji} & -x_{ji} & 0 \end{bmatrix},$$

$$\{\delta\}_{S4} = \{u_1 \ v_1 \ w_1 \ \theta_{x1} \ \theta_{y1} \ \theta_{z1} \ u_2 \cdots \theta_{z4}\}^T$$

Then we can express the displacement fields of the new four-node degenerated shell element with drilling DOF as follows.

$$\{u\} = [N]_{S8}[T]_{SR}\{\delta\}_{S4} \tag{8}$$

3. Assumed covariant strain method

Though in-plane performance can be improved by introducing the drilling DOF, transverse shear locking still remains to be solved. To circumvent the transverse shear locking, the assumed covariant strain method (Choi and Paik 1994) is incorporated into the present formulation. Two transverse shear strains are assumed to be linear in the natural coordinate system and tied to displacement based transverse shear strains at two end points. The interpolated shear strains are transformed back to the local coordinate system through tensor transformation.

3.1. Definition of the covariant strain components

We can obtain covariant displacement components u_α in the natural coordinate system by projecting displacement components u_i in the global Cartesian coordinate system onto the natural coordinate directions (ξ, η, ζ) as follows

$$u_\alpha = \frac{\partial x^i}{\partial \xi^\alpha} u_i \qquad (\alpha = \xi,\ \eta,\ \zeta) \tag{9}$$

where repeated indices imply summation over the range of 1 to 3 ($x^1=x$, $x^2=y$, $x^3=z$, $u_1=u$, $u_2=v$, $u_3=w$).

We also define the covariant strains corresponding to the covariant displacements as

$$\varepsilon_{\alpha\beta} = \frac{1}{2}(u_{\alpha,\beta} + u_{\beta,\alpha}) \qquad (\alpha = \xi,\ \eta,\ \zeta) \tag{10}$$

To avoid the transverse shear locking, we introduce assumed shear strain fields interpolated independently from the covariant shear strains at two end points as follows:

$$\bar{\gamma}_{\xi\zeta} = 2\bar{\varepsilon}_{\xi\zeta} = \frac{1+\eta}{2} 2\varepsilon_{\xi\zeta}\big|_{\xi=0,\eta=1} + \frac{1-\eta}{2} 2\varepsilon_{\xi\zeta}\big|_{\xi=0,\eta=-1} \tag{11a}$$

$$\bar{\gamma}_{\eta\zeta} = 2\bar{\varepsilon}_{\eta\zeta} = \frac{1+\xi}{2} 2\varepsilon_{\eta\zeta}\big|_{\xi=1,\eta=0} + \frac{1-\xi}{2} 2\varepsilon_{\eta\zeta}\big|_{\xi=-1,\eta=0} \tag{11b}$$

3.2. Substituted strain-displacement matrix

Since stress-strain relations are usually defined in the local Cartesian coordinates system, the assumed covariant transverse shear strains (Eqs. (11)) are transformed to the local Cartesian coordinates system by using the following formula:

$$\bar{\varepsilon}'_{i'j'} = \frac{\partial \xi^\alpha}{\partial x^{i'}} \frac{\partial \xi^\beta}{\partial x^{j'}} \bar{\varepsilon}_{\alpha\beta} \qquad (i',\ j' = x',\ y',\ z') \tag{12}$$

where repeated indices imply summation over the range of 1 to 3 ($\xi^1=\xi$, $\xi^2=\eta$, $\xi^3=\zeta$).

The other strain components can be obtained by differentiating the displacement fields in the typical manner. Then strain-displacement relations for the present element are given as

$$\{\varepsilon\} = \begin{Bmatrix} \varepsilon_{x'x'} \\ \varepsilon_{y'y'} \\ 2\varepsilon_{x'y'} \\ 2\bar{\varepsilon}_{x'z'} \\ 2\bar{\varepsilon}_{y'z'} \end{Bmatrix} = \begin{bmatrix} [B]_p \\ [B]_s \end{bmatrix} \{\delta\}_{S4} = [\bar{B}]\{\delta\}_{S4} \tag{13}$$

where $[B]_p$ is the in-plane strain-displacement matrix and $[B]_s$ is the transverse shear strain-displacement matrix.

4. Element stiffness matrix

We can obtain the element stiffness matrix in the same way as that of conventional degenerated shell elements with the strain-displacement matrix $[\bar{B}]$.

$$[K] = \int_v [\bar{B}]^T [D] [\bar{B}] \, dv$$
$$= \int_{-1}^{1} \int_{-1}^{1} \int_{-1}^{1} [\bar{B}]^T [D] [\bar{B}] |J| \, d\xi \, d\eta \, d\zeta \tag{14}$$

where $[D]$ is the elasticity matrix transformed to the local coordinate system and $\boldsymbol{J}$ is the jacobian matrix. We extend the formulation to deal with multi-layered structures by carrying out the through-thickness numerical integration. We consider it by substituting the variable ζ to ζ_k in the kth layer such that ζ_k varies from -1 to 1 in that layer (Panda and Natarajan 1981).

$$\zeta = -1 + \left[2 \sum_{j=1}^{k} h_j - h_k (1 - \zeta_k) \right] / t \tag{15}$$

$$d\zeta = \frac{h_k}{t} \cdot d\zeta_k \tag{16}$$

where t is the thickness of the shell and h_k is the thickness of the kth layer.

Substituting Eq. (15) and (16) into Eq. (14), we have

$$[K] = \sum_{j=1}^{NL} \int_{-1}^{1} \int_{-1}^{1} \int_{-1}^{1} [\bar{B}]^T [D] [\bar{B}] |J| \frac{h_k}{t} \, d\xi \, d\eta \, d\zeta_k \tag{17}$$

where NL is the number of layers in the element.

5. True rotation and penalty stiffness

Every term of the stiffness matrix is integrated by a 2×2 Gaussian quadrature. Two spurious modes are evoked in this element due to drilling DOF and subintegration. One is an equal rotation mode and the other is an hourglass mode.

The equal rotation mode occurs when the drilling DOF at all corner nodes have the same value and all translational displacements are zero. In practice, this mode is suppressed if the drilling DOF is constrained at least at one node. Nevertheless, this mode should be dealt with carefully in consideration of the true rotation of the continuum mechanics. The hourglass mode occurs when the stiffness terms are subintegrated. It is the same hourglass mode that occurs when an eight-node quadrilateral element is subintegrated. But this mode is not commutable and suppressed if more than two elements are used.

The equal rotation mode can be prevented by supplementing the stiffness derived from the penalty energy (Eq. (18)) of Kanok-Nukulchai (1979).

$$U_t = \alpha_t G \int_v \left[\alpha_3 - \frac{1}{2} \left(\frac{\partial v'}{\partial x'} - \frac{\partial u'}{\partial y'} \right) \right]^2 dv \tag{18}$$

where α_t is known as the torsional coefficient and G is shear modulus. If α_3 is the drilling rotation at any point on the midsurface, the variation is expressed as

$$\alpha_3 = \sum_{i=1}^{4} N_i \alpha_{3i} = \sum_{i=1}^{4} N_i \left(\overline{V}_{3i}^{x} \theta_{xi} + \overline{V}_{3i}^{y} \theta_{yi} + \overline{V}_{3i}^{z} \theta_{zi}\right) \tag{19}$$

where α_{3i} is the drilling rotation about the local z' axis at node i as shown in Fig. 1.

A one-point numerical integration should be used in evaluating the penalty energy in order to avoid over-constrained situation similar to shear locking. And α_t is chosen as 0.001. The constant α_t has very little influence on the results of plane problems. But inappropriate choice of α_t may result in errorneous solutions for structures with curved geometry and false drilling rotations. So, numerical experiments are considered to fix the value of α_t. The selected examples are Cook's membrane (8×8 mesh, Fig. 5), a hemispherical shell (16×16 mesh, Fig. 8), and a square slab (Fig. 10). It would be a reasonable choice since they are typical problems for evaluating membrane performance for distorted meshes, virtuality of the drilling rotation, and inextensional bending behavior of shell elements. The results of the test are shown in Fig. 3. It can be observed that α_t=0.001 is good for all examples.

The proposed element also utilizes the penalty energy (Eq. (20)) that was proposed by MacNeal and Harder (1988) for the hourglass mode.

$$P_2 = VG\,\delta\Theta_2^2 \tag{20}$$

where $\Theta_2 = (\alpha_{31} - \alpha_{32} + \alpha_{33} - \alpha_{34})/4$ and V is the volume of the element. The penalty parameter δ is chosen as 10^{-3}, which was recommended by MacNeal and Harder (1988).

6. Numerical examples

We solve a number of standard benchmark problems to investigate static performances of the proposed element. We also select several problems in addition to demonstrate

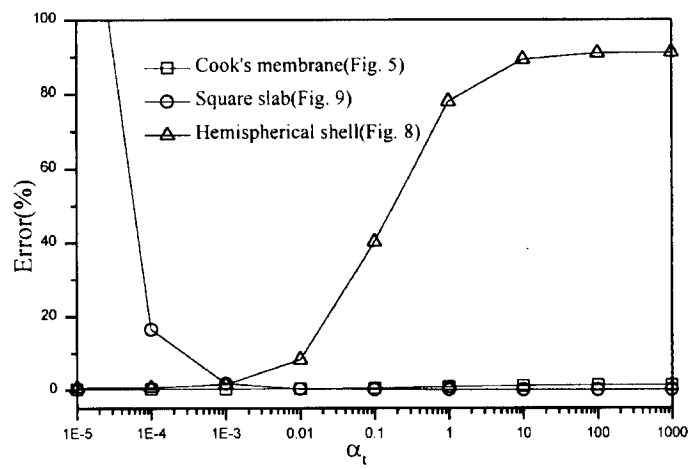

Fig. 3 Errors as a function of penalty parameter for selected problems

Table 1 Summary of elements used for comparison

Name	Element Description
AQR8	An assumed-stress hybrid four-node flast shell element with drilling DOF (Aminpour 1992)
QUADR	Four-node shell element with drilling DOF in MSC/NASTRAN (MacNeal *et al.* 1994)
MITC4	Four-node degenerated shell element based on assumed shear strain field (Bathe and Dvorkin 1986)
4-SRI	Four-node degenerated shell element with selectively reduced integration (Belytschko *et al.* 1989)
SQ4A	Four-node degenerated shell element based on assumed covariant strains (Choi and Paik 1994)

representability of true rotation and applicability to laminated composite materials. We make a list of shell elements to be compared in Table 1.

6.1. Patch tests

Patch tests described in MacNeal and Harder (1985) are performed. Boundary conditions and theoretical solutions for these tests are shown in Fig. 4. The drilling rotations on boundary nodes are set to be zero for the membrane patch test, which is naturally calculated from the prescribed displacement fields. The proposed element passes the membrane and bending patch tests with exact strains and stresses.

6.2. Cook's membrane problem

A trapezoidal membrane shown in Fig. 5 is used to test the sensitivities of finite elements to geometric distortions. The results for tip deflection are compared with the reference value of 23.91 obtained from a refined model (32×32 mesh). It can be observed in Table 2 that all

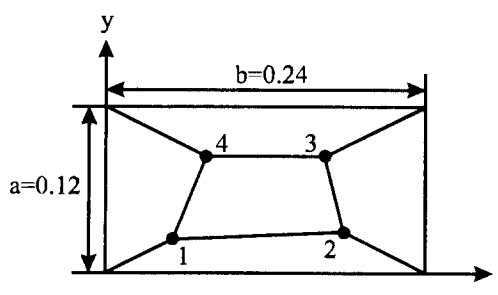

The position of nodes

Nodes	x	y
1	0.04	0.02
2	0.18	0.03
3	0.16	0.08
4	0.08	0.08

(a) Membrane plate patch test
Boundary conditions : $u = 10^{-3}(x + y/2)$, $v = 10^{-3}(x/2 + y)$
Theoretical solutions : $\varepsilon_{xx} = \varepsilon_{yy} = \gamma_{xy} = 10^{-3}$, $\sigma_{xx} = \sigma_{yy} = 1333.$, $\sigma_{xy} = 400.$

(b) Bending plate patch test
Boundary conditions : $w = 10^{-3}(x^2 + xy + y^2)/2$
Theoretical solution : $\theta_x = 10^{-3}(x/2 + y)$, $\theta_y = -10^{-3}(x + y/2)$
Bending moments per unit length : $M_x = M_y = 1.111 \times 10^{-7}$, $M_{xy} = 3.333 \times 10^{-8}$
Surface stresses : $\sigma_{xx} = \sigma_{yy} = 0.667$, $\sigma_{xy} = 0.200$

Fig. 4 The patch test

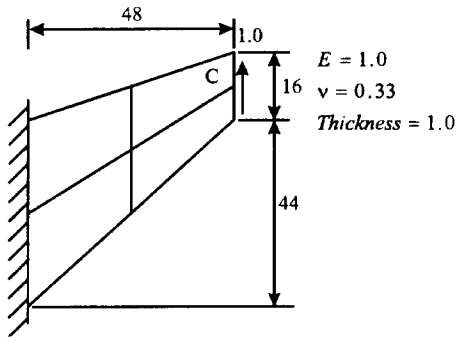

Fig. 5 Cook's membrane problem

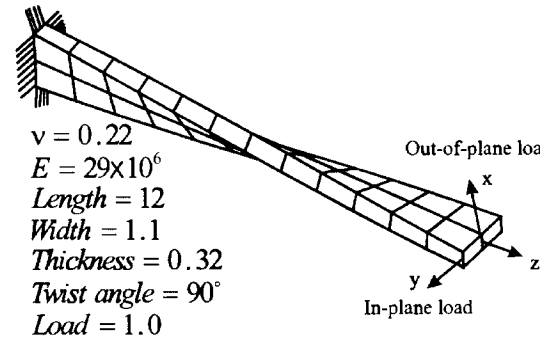

Fig. 6 Twisted cantilever beam

Table 2 Normalized solution for Cook's membrane

Nodes/Side	MITC4	SQ4A	AQR8	Present
3	0.495	0.724	0.930	0.890
5	0.765	0.906	0.979	0.965
9	0.924	0.974	–	0.997

Table 3 Normalized solutions for twisted beam

Load	In-plane		Out-of-plane	
Nodes/Side	3×13	5×25	3×13	5×25
4-SRI	0.995	0.998	0.924	0.976
MITC4	0.988	0.996	0.920	0.974
SQ4A	0.994	0.998	0.982	0.994
AQR8	0.991	–	1.093	–
Present	1.003	0.997	0.997	0.997

elements with drilling DOF are accurate and of high convergence rate.

6.3. A twisted cantilever

A cantilever beam of rectangular cross section, twisted 90° over its length, is subjected to a concentrated unit load at its free end as shown in Fig. 6. This problem tests the sensitivity of the elements to warping distortion. Both membrane and bending contributions are significant in this problem. The analytic solutions in the case of in-plane load and of out-of-plane load are 0.5424×10^{-2} and 0.1754×10^{-2}, respectively, as found in MacNeal and Harder (1985). The results of the normalized displacements are listed in Table 3. All elements show reasonable convergency to the analytic solutions. But the present element shows better results.

6.4. Scodelis-Lo cylindrical roof

The Scodelis-Lo cylindrical roof subjected to self-weight load is depicted in Fig. 7. Membrane contribution to deformation is significant in this problem. An analytic solution for the transverse displacement at the center of the edge (A), as reported by MacNeal and Harder

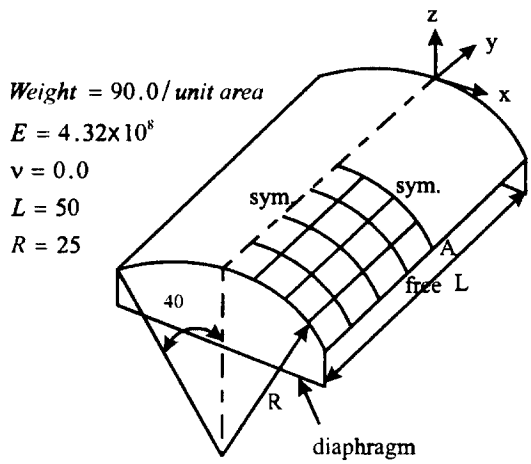

Fig. 7 Scodelis-Lo cylindrical roof

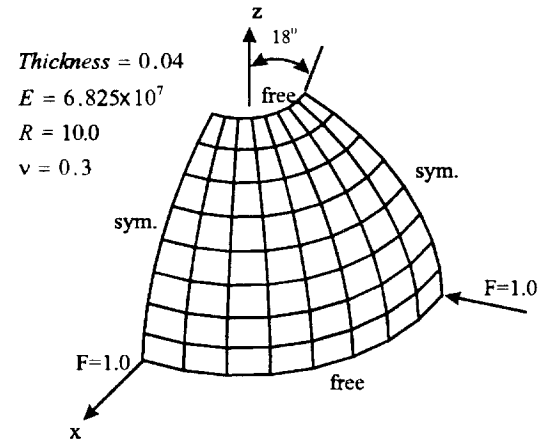

Fig. 8 Hemispherical shell

Table 4 Normalized solutions for Scodelis-Lo roof

Nodes/Side	4-SRI	QUADR	MITC4	SQ4A	AQR8	Present
5	0.964	1.055	0.944	1.044	1.021	1.052
9	0.984	1.009	0.973	1.002	1.003	1.007
17	0.999	–	0.989	0.995	–	0.998

(1985), is 0.3024. In consideration of symmetry of the structure, only a quarter of the roof is analyzed. Normalized values for the transverse displacement at A are listed in Table 4. All elements show good accuracy and high convergence rate for this problem.

6.5. A hemispherical shell with a hole

A quarter of the hemispherical shell with a hole is shown in Fig. 8. This problem is intended to check the element performance with rigid body rotations and in the case of near inextensional bending of a doubly curved shell. A reference solution for radial displacement at the loading points is 0.094, which is given in MacNeal and Harder (1985). The normalized displacements are shown in Table 5. Elements with drilling DOF show more or less slow convergence, though it seems not to be severe. It is well-known that the strain energy for this problem is almost bending energy. However, the membrane stiffness is much larger than the bending stiffness. So, any small amount of membrane-bending coupling strongly affects the stiffness of the shell. This membrane-bending coupling comes about by the coupling between the drilling rotation and the bending rotations by the changes in slope at element intersections (MacNeal and Harder 1988). The incorrect geometry representation causes the slow convergence for the present element.

6.6. Full hemispherical shell

An alternate form of the previous problem, the full hemispherical shell, is analyzed with the quarter model shown in Fig. 9. This problem is intended to check the element

Table 5 Results for hemispherical shell with a hole

Nodes/Side	QUADR	AQR8	Present
5	0.447	0.227	0.304
9	0.962	0.681	0.894
17	0.996	0.972	0.985

performance for the rigid body rotations and the near inextensional bending of a doubly curved shell with distorted meshes. The shell characteristics and the loading are exactly the same as in the previous example, but there is no hole on the top. A reference solution for radial displacement at the loading points is 0.0924, which is given in Flugge (1973). The normalized displacements are shown in Table 6. It is noted that for the same number of nodes per side fewer elements are used than in the previous example. The present element shows slow convergence for the same reason as in the previous example.

6.7. A square slab sustained by a column (Right angle beam-to-shell connection)

A horizontal square slab (first proposed and solved by Frey 1988) is sustained by a vertical central column and loaded by a resultant in-plane moment M_z=800, which is applied by horizontal forces or by concentrated moments, acting on four corners (see Fig. 10). The St. Venant stiffness of the column is J=790.55. The slab is discretized as in Fig. 10 so that the typical zero energy mode of rectangular elements might be avoided.

The displacements at the slab corner A for two loading cases are shown in Table 7. Since the slab is quite stiff as compared with the column, the overall rotation $\phi=u_A/c$ of the slab is

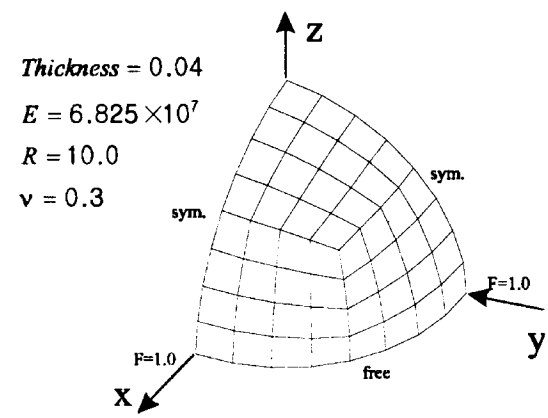

Fig. 9 Full hemispherical shell

Table 6 Results for full hemispherical shell

Nodes/Side	MITC4	SQ4A	Present
5	0.372	1.027	0.256
9	0.920	1.002	0.827
17	0.990	0.996	0.960

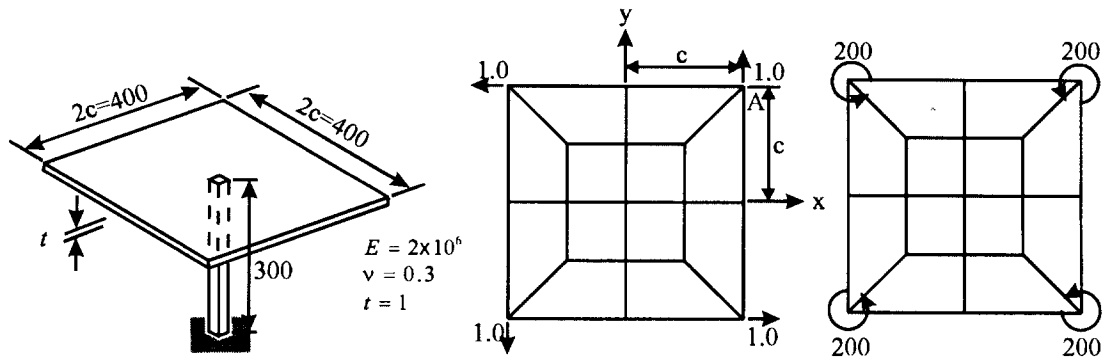

Fig. 10 Square slab to column connection

Table 7 Results of slab to column connection

	$-u_A=v_A$	$10^3\times\theta_{zA}$	$10^3\times\phi$
Couples of forces (Present)	0.080301	0.394662	0.401505
Concentrated moments (Present)	0.079015	0.394662	0.395075
Column top rotation angle (beam theory)		0.39466	

almost equal to the angle of twist of the column. The proposed element results in the exact solution for θ_{zA} while the displacement u_A shows a little discrepancy compared with the solution of $u_A=c\times\theta_{zA}=0.07893$.

6.8. A three-ply laminated square plate

A three-ply laminated square plate shown in Fig. 11 is carrying a uniformly distributed transverse load with simply supported boundaries. The plate has three layers of equal thickness. Each layer is assumed to be orthotropic. A 6×6 mesh is used in all computations. The nondimensionalized deflections at the center of the plate are presented in Table 8. Analytic solutions are found in Reddy (1992). The results for thin shells ($a/h > 10$) are closer to the analytic solutions than those for thick shells ($a/h < 10$). But, the errors for thick shells seem to be still in the tolerable range.

6.9. A cross-ply laminated spherical shell

A cross-ply laminated spherical shell shown in Fig. 12 is subjected to a uniformly

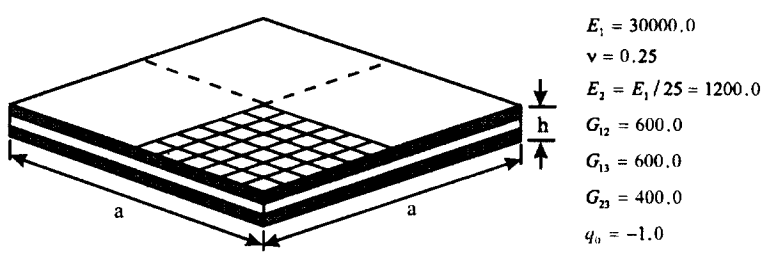

Fig. 11 Three-ply laminated square plate

Table 8 Nondimensionalized[a] deflections of three-layer cross-ply square plates under uniform load (0°/90°/0°, $h_j=h/3$)

a/h	2	4	10	20	50	100
Present	7.2149	2.5991	1.0238	0.7689	0.6949	0.6842
Analytic	7.7661	2.9091	1.0900	0.7760	0.6838	0.6705

a; $\bar{w} = (wh^3E_2/q_0a^4)\times10^2$

distributed transverse load. All layers are assumed to be orthotropic. All edges are simply-supported. Each edge is restricted to move in the direction of edge line but is free to move in the direction perpendicular to the edge line. Therefore, the edge which has originally a straight projection line on the xy-plane might not remain straight after deformation. Four corner points are fixed in consequence. Three kinds of ply construction are considered and all plies are of the same thickness. Because of double symmetry, only a quadrant is modeled. A 16×16 mesh is used in all cases. The nondimensionalized center deflections are presented in Table 9. Analytic solutions are referred to Reddy (1992). The proposed element shows good agreement with the analytic solutions.

6.10. A curved box girder

The last example is a curved box girder shown in Fig. 13. All parts including flanges, curved webs, and a diaphragm of the box girder are modeled by the present element. A half of the girder is modeled because of symmetry. Vertical deflections along the web lines of the flange are plotted in Fig. 14. The solutions are compared with the experimental results reported by Fam and Turkstra (1976). The present element exhibits fairly good performance even with a coarse mesh.

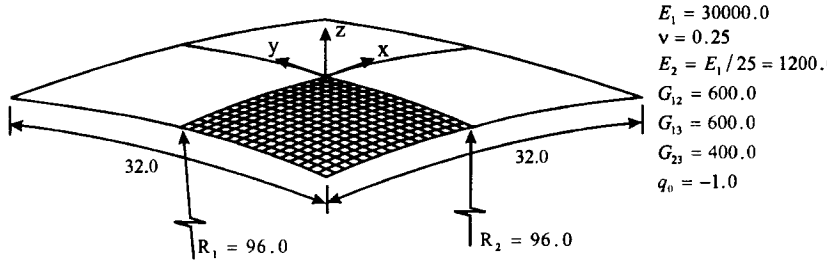

Fig. 12 Cross-ply laminated spherical shell (0°/90°, 0°/90°/0°, 0°/90°/90°/0°)

Table 9 Nondimensionalized[a] center deflections of spherical shell under uniformly distributed load

	0°/90°		0°/90°/0°		0°/90°/90°/0°	
	a/h=100	a/h=10	a/h=100	a/h=10	a/h=100	a/h=10
Present	0.6502	16.014	0.6453	8.9500	0.6454	8.8193
Analytic	0.6441	15.739	0.6224	9.1148	0.6246	9.1463

a; $\bar{w} = (wh^3E_2/q_0a^4)\times10^3$

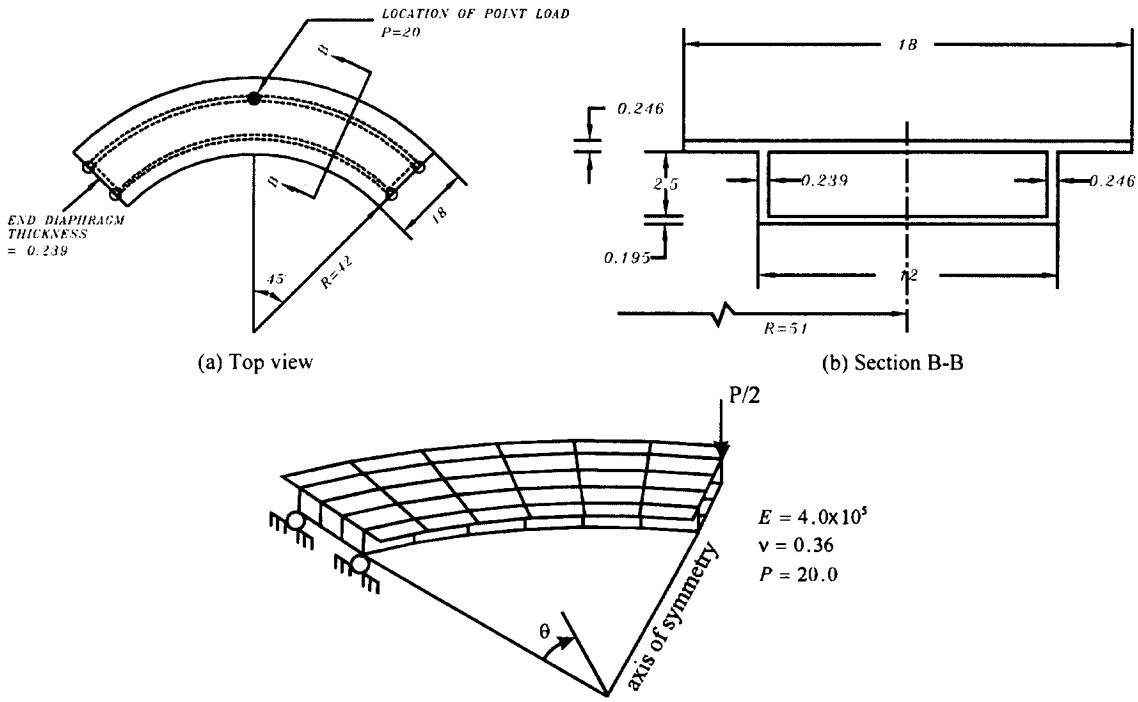

Fig. 13 Curved box girder (geometry and finite element model)

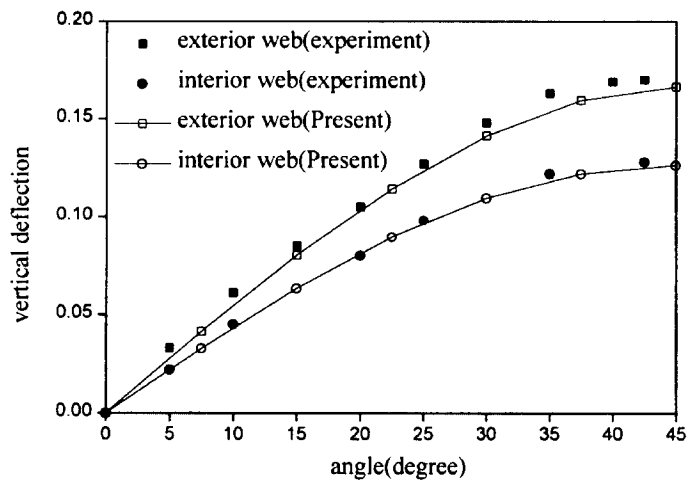

Fig. 14 Vertical deflection along the half span of box girder

7. Conclusions

A new four-node degenerated shell element with drilling DOF has been proposed. The element is free of locking and spurious modes. Numerical results show that the element is quite accurate and of proper convergence rate. It is also shown that the element is less

sensitive to element distortions and can be applied reliably to thin or moderately thick shell problems. Not only isotropic but also composite laminated structures are dealt with. True drilling rotations are calculated accurately. Stiffened or folded structures are handled more conveniently by the proposed element of six degrees of freedom per node.

References

Ahmad, S., Irons, B.M. and Zienkiewicz, O.C. (1970), "Analysis of thick and thin shell structures by curved finite elements", *Int. J. Numer. Methods Eng.*, **2**, 419-451.

Allman, D.J. (1984), "A compatible triangular element including vertex rotations for plane elasticity analysis", *Comp. Struct.*, **19**, 1-8.

Aminpour, M.A. (1992), "An assumed-stress hybrid 4-node shell element with drilling degrees of free dom", *Int. J. Numer. Methods Eng.*, **33**, 19-38.

Bathe, K.J. and Dvorkin, E.N. (1986), "A formulation of general shell elements-the use of mixed inter polation of tensorial components", *Int. J. Numer. Methods Eng.*, **22**, 697-722

Belytschko, T., Wong, B.L. and Stolarski, H. (1989), "Assumed strain stabilization procedure for 9-node Lagrange shell element", *Int. J. Numer. Methods Eng.*, **28**, 385-414.

Choi, C.K. and Paik, J.G. (1994), "An efficient four node degenerated shell element based on the as sumed covariant strain", *Structural Engineering and Mechanics, An Int. J.* **2**(1), 17-34.

Choi, C.K. and Lee, W.H. (1995), "Transition membrane elements with drilling freedom for local mesh refinements", *Structural Engineering and Mechanics, An Int. J.* **3**(1), 75-89.

Choi, C.K., Chung, K.Y. and Lee, N.H. (1996), "Three dimensional non-conforming 8-node solid elements with rotational degrees of freedom", *Structural Engineering and Mechanics, An Int. J.* **4**(5), 569-586.

Cook, R.D. (1994), "Four-node 'flat' shell element: Drilling degrees of freedom, membrane-bending coupling, warped geometry, and behavior", *Comput. Struct.*, **50**(4), 549-555.

Fam, A.R.M. and Turkstra, C. (1976), "Model study of horizontally curved box girder", *J. Engng. Struct. Div., ASCE,* **102**, ST5, 1097-1108.

Frey, F. (1989), "Shell finite elements with six degrees of freedom per node", *Analytical and. Computational Models of Shells, ASME, CED-Vol.* **3**, 291-316.

Flugge, W. (1973), *Stresses in Shells*, 2nd edition, Springer, Berlin.

Huang, H.C. and Hinton, E. (1986), "A new nine node degenerated shell element with enhanced mem brane and shear interpolation", *Int. J. Numer. Methods Eng.*, **22**, 73-92.

Ibrahimbegovic, A., Taylor, R.L. and Wilson, E.L. (1990), "A robust quadrilateral membrane finite element with drilling degrees of freedom", *Int. J. Numer. Methods Eng.*, **30**, 445-457.

Jang, J. and Pinsky, P.M. (1987), "An assumed covariant based 9-node shell element", *Int. J. Numer. Methods Eng.*, **24**, 2389-2411.

Kanok-Nukulchai, W. (1979), "A simple and efficient finite element for general shell analysis", *Int. J. Numer. Methods Eng.*, **14**, 179-200.

MacNeal, R.H. and Harder, R.L. (1985), "A proposed standard set of problems to test finite element accuracy", *Finite Elements. Anal. Des.*, **1**, 3-20.

MacNeal, R.H. and Harder, R.L. (1988), "A refined four-noded membrane element with rotational degrees of freedom", *Comp. Struct.*, **28**, 75-84.

MacNeal, R.H. (1994), *Finite Elements: Their Design and Performance*, Marcel Dekker, New York.

Panda, S. and Natarajan, R. (1981), "Analysis of laminated composite shell structures by finite element method", *Comp. Struct.*, **14**, 225-230.

Park, K.C. and Stanley, G.M. (1986), "A curved C shell element based on assumed natural-coordinate strains", *J. of Applied Mechanics, ASME,* **53**, 278-290.

Reddy, J.N. (1992), *Energy and Variational Methods in Applied Mechanics*, John Wiley & Sons, New York.

Sze, K.Y. and Ghali, A. (1993), "A hybrid brick element with rotational degrees of freedom", *Comput. Mech.*, **12**, 147-163.

Sze, K.Y., Sim, Y.S. and Soh, A.K. (1997), "A hybrid stress quadrilateral shell element with full rotational D.O.F.s", *Int. J. Numer. Methods Eng.*, **40**, 1785-1800.

Taylor, R.L., Simo, J.C., Zienkiewicz, O.C. and Chan, A.C. (1986), "The patch test: A condition for assessing finite element convergence", *Int. J. Numer. Methods Eng.*, **22**, 39-62.

Yunus, S.M., Pawlak, T.P. and Cook, R.D. (1991), "Solid elements with rotational degrees of free dom: Part 1-Hexahedron elements", *Int. J. Numer. Methods Eng.*, **31**, 573-592.

Zienkiewicz, O.C., Taylor, R.L. and Too, J.M. (1971), "Reduced integration technique in general analysis of plates and shells", *Int. J. Numer. Methods Eng.*, **3**, 275-290.